TU Delft

Delft University of Technology

Large, low-field and reversible magnetostrictive effect in MnCoSi-based metamagnet at room temperature

Liu, Jun; Gong, Yuanyuan; Zhang, Fengqi; You, Yurong; Xu, Guizhou; Miao, Xuefei; Xu, Feng

DOI
10.1016/j.jmst.2020.11.011

Publication date
2021

Document Version
Final published version

Published in
Journal of Materials Science and Technology

Citation (APA)
Liu, J., Gong, Y., Zhang, F., You, Y., Xu, G., Miao, X., & Xu, F. (2021). Large, low-field and reversible magnetostrictive effect in MnCoSi-based metamagnet at room temperature. *Journal of Materials Science and Technology*, *76*, 104-110. https://doi.org/10.1016/j.jmst.2020.11.011

Important note
To cite this publication, please use the final published version (if applicable).
Please check the document version above.

Copyright
Other than for strictly personal use, it is not permitted to download, forward or distribute the text or part of it, without the consent of the author(s) and/or copyright holder(s), unless the work is under an open content license such as Creative Commons.

Takedown policy
Please contact us and provide details if you believe this document breaches copyrights.
We will remove access to the work immediately and investigate your claim.

This work is downloaded from Delft University of Technology.
For technical reasons the number of authors shown on this cover page is limited to a maximum of 10.

Journal of Materials Science & Technology 76 (2021) 104–110

Contents lists available at ScienceDirect

Journal of Materials Science & Technology

journal homepage: www.jmst.org

Research article

Large, low-field and reversible magnetostrictive effect in MnCoSi-based metamagnet at room temperature

Jun Liu [a], Yuanyuan Gong [a,*], Fengqi Zhang [b], Yurong You [a], Guizhou Xu [a], Xuefei Miao [a], Feng Xu [a,*]

[a] MIIT Key Laboratory of Advanced Metallic and Intermetallic Materials Technology, School of Materials Science and Engineering, Nanjing University of Science and Technology, Nanjing 210094, China
[b] Fundamental Aspects of Materials and Energy (FAME), Faculty of Applied Sciences, Delft University of Technology, Mekelweg 15, 2629 JB Delft, the Netherlands

ARTICLE INFO

Article history:
Received 16 June 2020
Received in revised form 6 August 2020
Accepted 4 September 2020
Available online 6 November 2020

Keywords:
Magnetostrictive effect
Magnetoelastic transition
Tricritical point
Reversibility
MnCoSi alloy

ABSTRACT

TiNiSi-type MnCoSi-based alloys show large magnetostriction during the magnetic-field-induced metamagnetic transition. However, the high critical field required to drive the transition directly hinders their potential applications. In this work, we systematically investigate the tricritical behavior and magnetostrictive effect in substituted MnCoSi alloys. Replacing Si with Sb or In, Co with Fe or Cu, and Mn with Co, which can simultaneously reduce the critical field and the temperature of tricritical point, are explored. Among the substituted MnCoSi alloys, $Mn_{0.983}Co_{1.017}Si$ displays a temperature of a tricritical point of 250 K and a room-temperature critical field of 0.60 T, which is the lowest up to now. Profited from these optimizations, a large reversible magnetostrictive effect under low field is successfully realized at room temperature. In a field of 1 T, the magnetostriction of $Mn_{0.983}Co_{1.017}Si$ alloy is close to 1000 ppm. Besides, a strong relation between critical field and valence electron concentration is revealed in the transition-metal-substituted MnCoSi alloys. Our work greatly enhances the low-field magnetostrictive performance of MnCoSi-based alloys and make them be of interest in potential applications.

© 2020 Published by Elsevier Ltd on behalf of The editorial office of Journal of Materials Science & Technology.

1. Introduction

Magnetostrictive effect, expressing as a strain response under a magnetic field, is an intrinsic phenomenon for almost all ferromagnets [1–3]. The giant magnetostrictive materials, such as $Tb_{0.3}Dy_{0.7}Fe_2$ (Terfenol-D) and $Fe_{100-x}Ga_x$ alloys [2,4–8], have been widely used in active vibration control, sensors, actuators and transducers [9,10]. Recently, the magnetic-phase-transition alloys are also found to change their shapes when placed in a magnetic field, an effect referred as magnetostrain [11–17]. This large magnetostrain is originated from the magnetic-field-induced first-order magnetostructural or magnetoelastic transformation, opening up an alternative way to seek new magnetomechanical materials [11–17]. However, due to the first-order nature of the transition, the obtained magnetostrain is always accompanied by large irreversibility featuring an obvious magnetic hysteresis [11–17]. It will cause functionally fatigue when field oscillation is applied. Therefore, towards the application of magnetic-phase-transition alloys in magnetomechanical devices, it is essential to realize reversible magnetostrain, namely magnetostriction.

The unique tricritical behavior of TiNiSi-type MnCoSi alloy provides possibilities to tame the reversibility of the magnetostriction during the field-induced transition [18–22]. The tricritical behavior in MnCoSi alloy can be understood as the temperature-dependent metamagnetic transition from an incommensurate helical antiferromagnetic state to a high magnetization state below Néel temperature (T_N =381 K) [18–25]. With decreasing the temperature, the nature of this metamagnetic transition changes from second-order to first-order. Thus, a tricritical point which is defined as the onset of hysteresis can be observed in the Field-Temperature diagram [18–25]. Interestingly, no matter the transition is first-order or second-order, a sizeable lattice distortion, which is the source of the large magnetostriction [18–22], is always accompanied by. For stoichiometric MnCoSi alloy (its isothermal magnetization (M-B) curves are shown in Fig. 1(a)), the temperature of tricritical point (T_{tri}) is 300 K and the critical field (B_{cri}) required to drive the transition is about 2.5 T at room temperature. Thus, to obtain a large magnetostrain at room tem-

* Corresponding authors.
E-mail addresses: gyy@njust.edu.cn (Y. Gong), xufeng@njust.edu.cn (F. Xu).

https://doi.org/10.1016/j.jmst.2020.11.011
1005-0302/© 2020 Published by Elsevier Ltd on behalf of The editorial office of Journal of Materials Science & Technology.

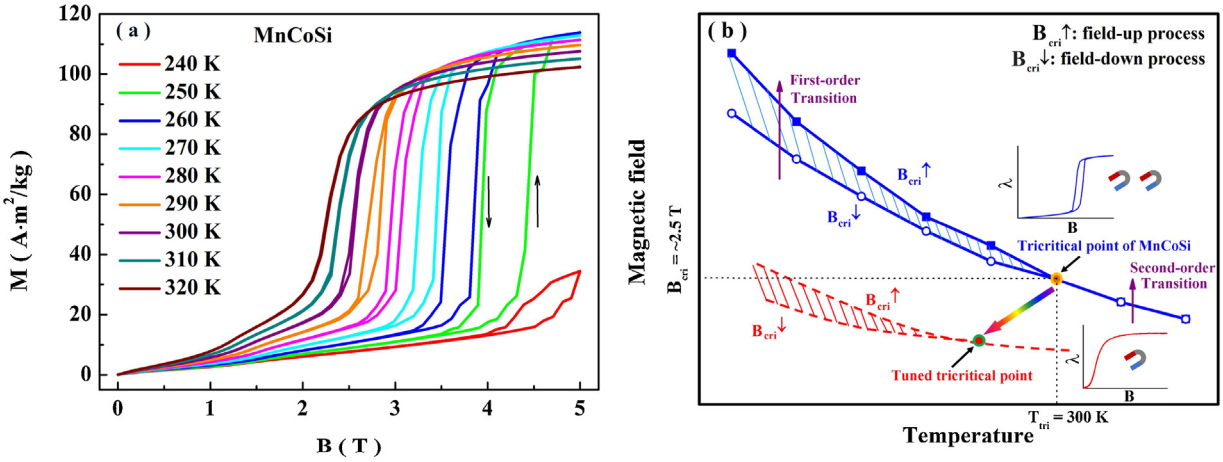

Fig. 1. (a) M-B curves for stoichiometric MnCoSi alloy. (b) Field-Temperature diagram. Blue lines: tricritical behavior in stoichiometric MnCoSi alloy. Red lines: tricritical behavior with reduced T_{tri} and B_{cri}. $B_{cri}\uparrow$ and $B_{cri}\downarrow$ represent the values of critical field in field-up and field-down processes, respectively. The magnetostriction curves at room temperature are also included as insets.

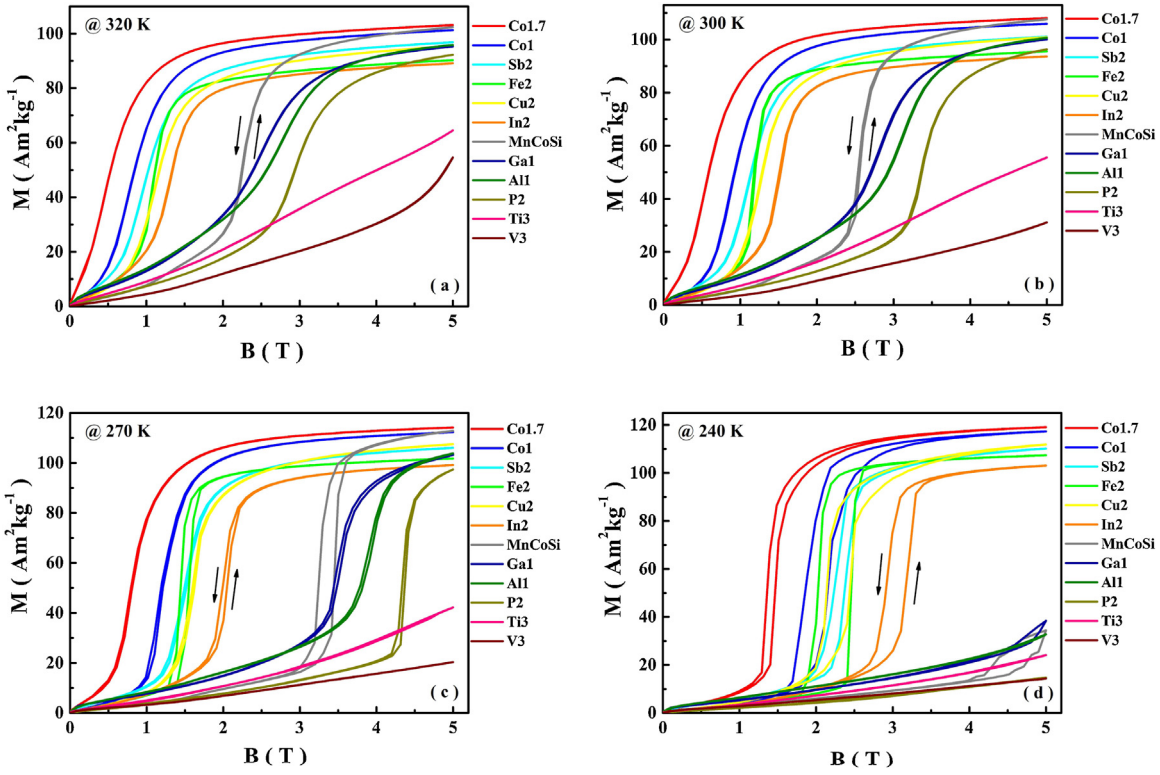

Fig. 2. *M-B* curves of MnCoSi-based alloys at 320 K (a), 300 K (b), 270 K (c) and 240 K (d).

perature, a high magnetic field should be applied. Furthermore, due to the first-order nature of this magnetic-field-induced transition, the obtained magnetostrain is accompanied by obvious hysteresis. However, when both T_{tri} and B_{cri} decrease, the metamagnetic transition turns into a second-order one at room temperature and a reduced magnetic field can trigger the transition [19–21]. In that case, large reversible magnetostriction under a low field can be expected in MnCoSi-based alloys. The specific schematic is illustrated in Fig. 1(b).

Some methods have been proposed to tune the tricritical behavior of MnCoSi alloy. Replacing Si with Ge [22,23,26] or B [20], Co with Ni [18,24], Mn with Fe [24,27], introducing Si-vacancy [19] and applying hydrostatic pressure [28] have been reported to reduce B_{cri} in the condition of that T_{tri} decreases. However, up to now, a way that can efficiently suppress B_{cri} is still absent. To the best of our knowledge, the lowest B_{cri} in the MnCoSi-based samples by slow-cooling heat treatment appears in $MnCo_{0.95}Ni_{0.05}Si$ and $MnCoSi_{0.98}B_{0.02}$, but still as high as 0.80 T at room temperature. It results in low magnetostriction under a field of 1 T [20,24]. Therefore, in the condition of that T_{tri} is below room temperature, B_{cri} should be further reduced so that the low-field magnetostriction can be enhanced.

In this study, we systematically investigate the effect of trace element substitutions on the tricritical behavior based on the atomic occupancy rule in Mn*MX* (*M* = Co or Ni, *X* = Si or Ge) alloys: the transition-metal atom with more valence electrons preferably occupies the Co site; while the transition-metal atom with less valence electrons preferably occupies the Mn site; the main-group

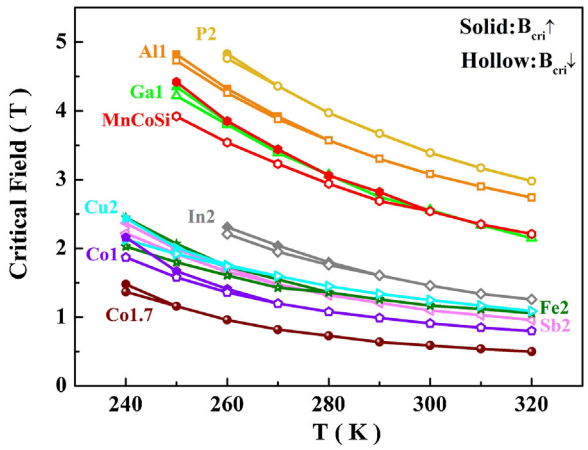

Fig. 3. Field-temperature diagram of MnCoSi-based alloys.

atom intends to occupy the Si site [29–32]. Replacing Si with Sb or In, Co with Fe or Cu, and Mn with Co are found to reduce B_{cri} and T_{tri} simultaneously. Replacing Mn with Co displays the largest reduction rate of B_{cri} by doping content. In $Mn_{0.983}Co_{0.017}Si$ alloy, the room-temperature B_{cri} reaches 0.60 T and the T_{tri} is around 250 K. It guarantees a large reversible magnetostriction under 1 T at ambient environment.

2. Experimental

Polycrystalline $Mn_{1-x}T_xCoSi$ (T = Ti and V), $Mn_{1-x}Co_{1+x}Si$, $MnCo_{1-x}Y_xSi$ (Y = Fe and Cu) and $MnCoSi_{1-x}Z_x$ (Z = Al, Ga, P, In, Sn and Sb) were prepared by arc-melting the appropriate amounts of high purity (≥ 99.9 %) raw materials for three times under argon atmosphere. The doping content x is chosen to be lower than 3% because a handful of dopant atoms can obviously affect the metamagnetic behavior and a larger x may bring about the impurity phases in some substituted MnCoSi alloys. In order to fully release the inner stress, the ingots sealed in vacuum quartz tubes were annealed at 1123 K for 60 h, and then slowly cooled down to room temperature in 72 h.

Crystal structures were identified by X-ray diffraction (XRD, Bruker D8 Advance) with CuK_α radiation at room temperature. M-B curves were measured by a physical property measurement system (PPMS, Quantum Design Dynacool) with a vibrating sample magnetometer module. At each target temperature, the data were recorded in the magnetic-field-up and -down processes. Then the temperature was increased by 10 K and the M-B loop was measured again. The microstructure of the bulk sample after solidification was observed by scanning electron microscope (SEM, FEI Quanta 250 F). The thermal expansion property was measured by thermal mechanical analyzer (TMA, Netzsch F3). Magnetostriction measurement was carried out using a standard strain gauge technique on PPMS.

3. Results

3.1. Structural information

The isostructural alloying principle is often adopted to manipulate the properties of materials by alloying two compounds with the same crystal structure [30,31,33–35]. Since MnCoP, TiCoSi, VCoSi and Co_2Si alloys crystallize in TiNiSi-type orthorhombic structure [36,37], a high-level introduction of P into Si site and Ti, V or Co into Mn site would not induce impurity phases. It is also reported that $MnCo_{1-x}Fe_xSi$ alloys can maintain TiNiSi-type structure when x reaches 0.4 [38,39]. Nevertheless, even if the doping content is lower than 3%, the metamagnetic transition can be obviously affected. Therefore, the compounds with the compositions of $MnCoSi_{0.98}P_{0.02}$ (P2), $Mn_{0.97}Ti_{0.03}CoSi$ (Ti3), $Mn_{0.97}V_{0.03}CoSi$ (V3), $MnCo_{0.98}Fe_{0.02}Si$ (Fe2), $Mn_{0.99}Co_{1.01}Si$ (Co1) and $Mn_{0.983}Co_{1.017}Si$ (Co1.7) are investigated in this work. For the other element substitutions, such as replacing Co with Cu and Si with Al, Ga, In or Sb, due to the limited solid solubility, impurity phases can be obviously traced when the doping content reaches 2 %–3 %. The maximum doping content is 1% for Al and Ga substitution, and 2% for the other three. Thus, the experimental results of $MnCoSi_{0.99}Al_{0.01}$ (Al1), $MnCoSi_{0.99}Ga_{0.01}$ (Ga1), $MnCoSi_{0.98}In_{0.02}$ (In2), $MnCoSi_{0.98}Sb_{0.02}$ (Sb2) and $MnCo_{0.98}Cu_{0.02}Si$ (Cu2) alloys are shown here.

Since Mn atom carries the major magnetic moment, the nearest Mn-Mn separation (d, shown in Fig. S1(a) in Supplementary Material) determines the magnetic ground state of Mn-based orthorhombic magnet in *Pnma* space group [18,40,41]. It is reported that with the increase of d, the exchange interaction changes from the nonlinear antiferromagnetic to ferromagnetic [40,41]. Thus, increasing d will stabilize the high magnetization state, leading to the decrease of B_{cri} [42]. The structural information of the samples mentioned above is obtained according to the Rietveld refinement of XRD data of powdered samples at room temperature (listed in Table 1 and shown in Fig. S1 in Supplementary material). It can be found that Ti3, V3, Al1, Ga1 and P2 exhibit reduced d relative to MnCoSi alloy, while Co1.7, Fe2, Cu2, In2 and Sb2 possess enlarged one. It suggests that reduced B_{cri} can be fulfilled in the latter five samples.

3.2. The metamagnetic transition and tricritical behavior

To investigate the metamagnetic transitions in all the samples, the M-B curves were measured with a maximum magnetic field of 5 T (shown in Fig. S2 in Supplementary material). For simplicity, the M-B curves at 320, 300, 270 and 240 K are summarized in Fig. 2(a)–(d). In the temperature range of 240−320 K, the M-B curves of Ti3 and V3 continuously increase without any obvious change of the slope, demonstrating that replacing Mn with Ti or V will increase B_{cri} so that a magnetic field of 5 T is not high enough to drive the metamagnetic transition. For P2, Al1 and Ga1, although the metamagnetic transition can be observed above 270 K (Fig. 2(a)–(c)), the M-B curves of these three samples lie at the right side of that of MnCoSi alloy. The values of B_{cri} are 3.39, 3.07 and 2.57 T for P2, Al1 and Ga1 at 300 K, respectively. Here, B_{cri} is denoted as the point where the magnetization is 50 % of its saturation value [19,27]. Further decreasing the temperature will increase B_{cri} [18–20,42] and thus the metamagnetic transition disappears at 240 K (Fig. 2(d)). This phenomenon suggests that replacing Si with P, Al or Ga will also increase B_{cri}.

Different from above-mentioned five samples, Co1, Fe2, Cu2, In2 and Sb2 possess reduced B_{cri} because their M-B curves are located on the left side of that of MnCoSi alloy. The corresponding values of B_{cri} are 0.91, 1.11, 1.17, 1.25 and 1.46 T for Co1, Sb2, Fe2, Cu2 and In2 at 300 K, respectively. The values of room-temperature B_{cri} of reported MnCoSi-based alloys are also listed in Table 2 for comparison [19,20,23,24,26,27]. To exclude the influence of magnetic inhomogeneity caused by quenching [43], only the data of MnCoSi-based alloys prepared by slow-cooling are shown here. It is worth noting that replacing 1% Mn with Co can lead to a sharp decrease of room-temperature B_{cri} by 1.59 T. As we know, it is the most efficient way to reduce B_{cri} up to now. To maximumly reduce B_{cri} by Co-substitution, the doping content is increased to 1.7 %. In that case, a low room-temperature B_{cri} of 0.60 T is obtained (Fig. 2(b) and Table 2). With further increasing the doping content to 2%, the room-temperature metamagnetic transition will disappear and the sample becomes ferromagnetic-like (Fig. S3 in Supplementary material). In summary, with the shrinkage of d, Ti, V, P, Al and Ga

Table 1
Lattice parameters *a*, *b* and *c*, unit-cell volume *V*, nearest Mn-Mn distance *d* and atomic occupancy sites for studied MnCoSi-based samples. The space group is *Pnma* and Wyckoff position is 4c (*x*, 1/4, *z*).

Samples	*a* (Å)	*b* (Å)	*c* (Å)	*V* (Å^3)	*d* (Å)	x_{Mn}/z_{Mn}	x_{Co}/z_{Co}	x_{Si}/z_{Si}	R_{wp}/R_p (%)
Ti3	5.8918(9)	3.6924(5)	6.8672(5)	149.40(5)	3.075	0.0150(2)/0.1785(5)	0.1536(8)/0.5652(2)	0.7703(8)/0.6199(7)	5.37/3.69
V3	5.8891(5)	3.6909(1)	6.8674(3)	149.27(1)	3.065	0.0164(4)/0.1776(4)	0.1537(1)/0.5586(6)	0.7729(7)/0.6178(8)	5.79/3.97
Al1	5.8793(1)	3.6926(6)	6.8651(8)	149.04(4)	3.070	0.0157(1)/0.1781(2)	0.1549(1)/0.5571(2)	0.7620(2)/0.6260(2)	6.37/4.42
Ga1	5.8851(2)	3.6961(2)	6.8714(2)	149.47(1)	3.077	0.0166(3)/0.1784(3)	0.1632(1)/0.5638(7)	0.7623(8)/0.6259(1)	6.38/4.29
P2	5.8858(1)	3.6906(1)	6.8646(2)	149.11(1)	3.072	0.0167(9)/0.1783(4)	0.1578(6)/0.5602(8)	0.7594(6)/0.6277(1)	5.30/3.75
MnCoSi	5.8817(3)	3.6948(7)	6.8700(4)	149.30(4)	3.087	0.0140(3)/0.1796(2)	0.1553(6)/0.5604(1)	0.7426(6)/0.6231(1)	6.07/4.15
Co1.7	5.8614(8)	3.6985(2)	6.8736(7)	149.01(4)	3.118	0.0230(1)/0.1815(3)	0.1573(3)/0.5564(7)	0.7643(1)/0.6268(9)	4.8/3.57
Fe2	5.8718(7)	3.6983(4)	6.8775(9)	149.35(5)	3.121	0.0187(8)/0.1820(4)	0.1596(6)/0.5635(6)	0.7688(3)/0.6261(9)	5.32/3.87
Cu2	5.8458(2)	3.6811(3)	6.8477(4)	147.36(2)	3.100	0.0207(1)/0.1810(6)	0.1619(1)/0.5637(1)	0.7354(2)/0.6231(3)	5.70/3.82
In2	5.8634(2)	3.6917(4)	6.8623(3)	148.54(3)	3.099	0.0173(8)/1.8072(1)	0.1589(1)/0.5670(3)	0.7660(3)/0.6264(9)	4.28/3.36
Sb2	5.8423(1)	3.6863(2)	6.8495(4)	147.51(2)	3.132	0.0290(7)/0.1832(5)	0.1586(4)/0.5530(2)	0.7245(5)/0.6286(1)	4.79/3.31

Table 2
The temperature of tricritical point (T_{tri}) and the critical field (B_{cri}) for driving the metamagnetic transition at room temperature in MnCoSi-based alloys after the heat treatment of slow cooling.

samples	B_{cri} @ RT (T)	T_{tri} (K)	References	Samples	B_{cri} @ RT (T)	T_{tri} (K)	References
Al1	3.07	280	This work	Ga1	2.57	280	This work
P2	3.39	270	This work	Fe2	1.17	280	This work
Cu2	1.25	270	This work	In2	1.46	290	This work
Sb2	1.11	270	This work	Co1	0.91	270	This work
Co1.7	0.60	250	This work	MnCoSi	2.54	300	This work
$MnCoSi_{0.98}$	1.30	260	[19]	$MnCo_{0.95}Ni_{0.05}Si$	0.80	250	[24]
$MnCoSi_{0.98}B_{0.02}$	0.8	270	[20]	$Mn_{0.95}Fe_{0.05}CoSi$ [a]	–	180	[27]
$MnCoSi_{0.92}Ge_{0.08}$	1.50	262	[23]	$MnCoSi_{0.95}Ge_{0.05}$ [b]	1.60	–	[26]

[a] $Mn_{0.95}Fe_{0.05}CoSi$ alloy is ferromagnetic-like at room temperature, thus no metamagnetic transition is observed.
[b] The T_{tri} of $MnCoSi_{0.95}Ge_{0.05}$ was not shown in Ref. [26].

substitutions increase B_{cri}, while due to the increase of *d*, Co, Fe, Cu, In and Sb-substituted MnCoSi alloys exhibit reduced B_{cri}.

Temperature dependence of B_{cri} in field-up and -down processes ($B_{cri}\uparrow$ and $B_{cri}\downarrow$) are summarized in the Field-Temperature diagram, as shown in Fig. 3. With the temperature decreases to be lower than T_{tri}, the metamagnetic transition changes from second-order to first-order, presenting as the onset of inconsistency between $B_{cri}\uparrow$ and $B_{cri}\downarrow$. As listed in Table 2, all the studied samples show reduced T_{tri} relative to that of MnCoSi alloy. Combing with the above-mentioned analysis, it can be said that Co1.7, Co1, Fe2, Cu2, In2 and Sb2 possesses both reduced B_{cri} and T_{tri}. Therefore, large reversible magnetostriction is promising to be fulfilled in these samples at room temperature.

3.3. Magnetostrictive effect

Due to the temperature gradient between the molten alloy and the water-cooled copper crucible, texture forms along the solidification direction in these MnCoSi-based samples. Here, we took Co1.7 as an example and show its SEM image of cross-section in Fig. 4(a). Columnar grains can be observed. A similar phenomenon has also been reported in Ni-Mn-based Heusler alloys prepared by arc melting [14,44]. As reported before [18,20], the polycrystalline MnCoSi with preferred orientation exhibits anisotropic thermal expansion behavior. As shown in Fig. 4(b), both Cu2 and Co1.7 display negative (positive) thermal expansion in the direction perpendicular (parallel) to the columnar grain below T_N. By comparing this result with the thermal expansion data of MnCoSi along *a*, *b* and *c* axes in Ref. [18], it can be found that the thermal expansion along the solidification direction is similar with that along *b* or *c* axis. However, when vertical, an *a*-like behavior can be observed. This phenomenon suggests that *a* axis inclines to be perpendicular to the solidification direction. It is consistent with the results obtained in B-substituted MnCoSi [20].

The magnetostriction curves ($\lambda = \Delta L/L$) of In2, Cu2, Sb2 and Co1.7 were measured at 270, 280, 290 and 300 K. Due to the existence of texture, the anisotropic magnetostrictive effect is observed. Here, $\lambda//$ and $\lambda\perp$ denote the magnetostriction along and perpendicular to the solidification direction, respectively. As shown in Fig. 5, with increasing the magnetic field to be higher than B_{cri}, both $\lambda//$ and $\lambda\perp$ change significantly. This behavior indicates that the obtained magnetostriction is derived from the magnetic-field-induced metamagnetic transition. As reported in Ref. [24], the metamagnetic transition in MnCoSi alloy is accompanied by the shrinkage along *a* axis and the elongation along *b* and *c* axes. The absolute value of the shrinkage along *a* axis is larger than the expansion along the other two axes [24]. Since the *a* axis is perpendicular to the solidification direction, $\lambda\perp$is negative and $\lambda//$ is positive. The values of magnetostriction under 1 and 2 T are summarized in Table 3. At 270 K, the values of $\lambda//$ ($\lambda\perp$) are 580, 1322, 1270 and 1690 ppm (-529, -1317, -1856 and -1184 ppm) in 2 T for In2, Cu2, Sb2 and Co1.7, respectively. The relatively low magnetostriction of In2 is ascribed to the relatively high B_{cri} (> 2 T) at 270 K and thus only part of the sample experiences the magnetic-field-induced metamagnetic transition (Fig. S2(j) in Supplementary Material). With increasing the temperature to 300 K, a field of 2 T is high enough to complete the metamagnetic transition in these four samples. The corresponding values of $\lambda//$ ($\lambda\perp$) are 969, 983, 917 and 1186 ppm (-935, -988, -1348 and -792 ppm) for In2, Cu2, Sb2 and Co1.7, respectively. Owing to the large B_{cri} at room temperature (2.5 T), the stoichiometric MnCoSi displays low magnetostriction: 95 ppm for $\lambda//$ and -119 ppm for $\lambda\perp$ under 2 T at 300 K (Fig. S4 in Supplementary material). These values are much smaller than those of In2, Cu2, Sb2 and Co1.7. Profit from the reduction of T_{tri}, the magnetostrictive effect of In2, Cu2, Sb2 and Co1.7 at room temperature is originated from the reversible second-order metamagnetic transition with hysteresis-free behavior. Hence, the reversibility of the magnetostrictive effect is greatly improved.

More importantly, since Co1.7 exhibits both the lowest room-temperature B_{cri} and T_{tri}, large reversible magnetostriction under a low magnetic field at room temperature is promising to be fulfilled. For Co1.7, the values of $\lambda//$ and $\lambda\perp$ under 1 T at 300 K reach 993 and

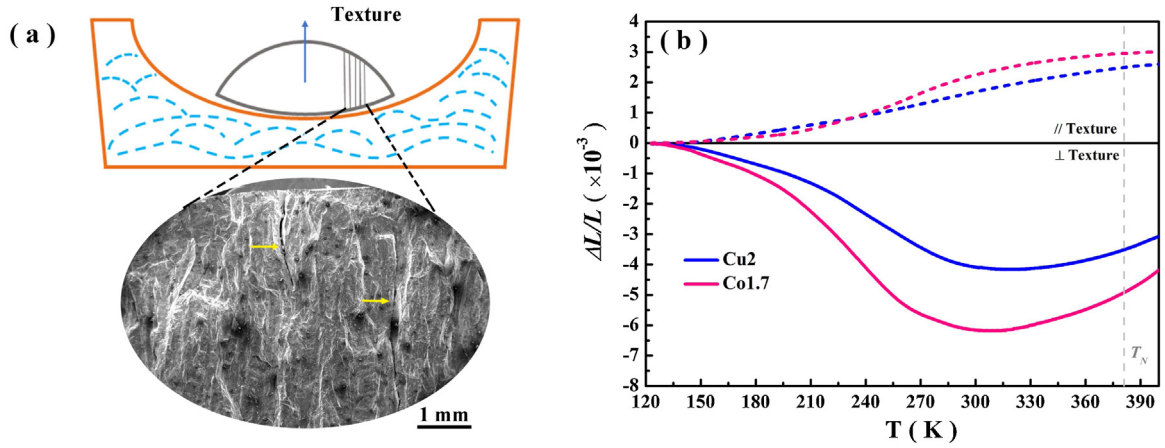

Fig. 4. (a) The schematic on the formation of texture in MnCoSi alloy and the SEM image of the cross-section of Co1.7. The yellow arrows indicate the spontaneous cracks. (b) The temperature dependence of thermal expansion of Co1.7 and Cu2 in the direction parallel and perpendicular to the texture.

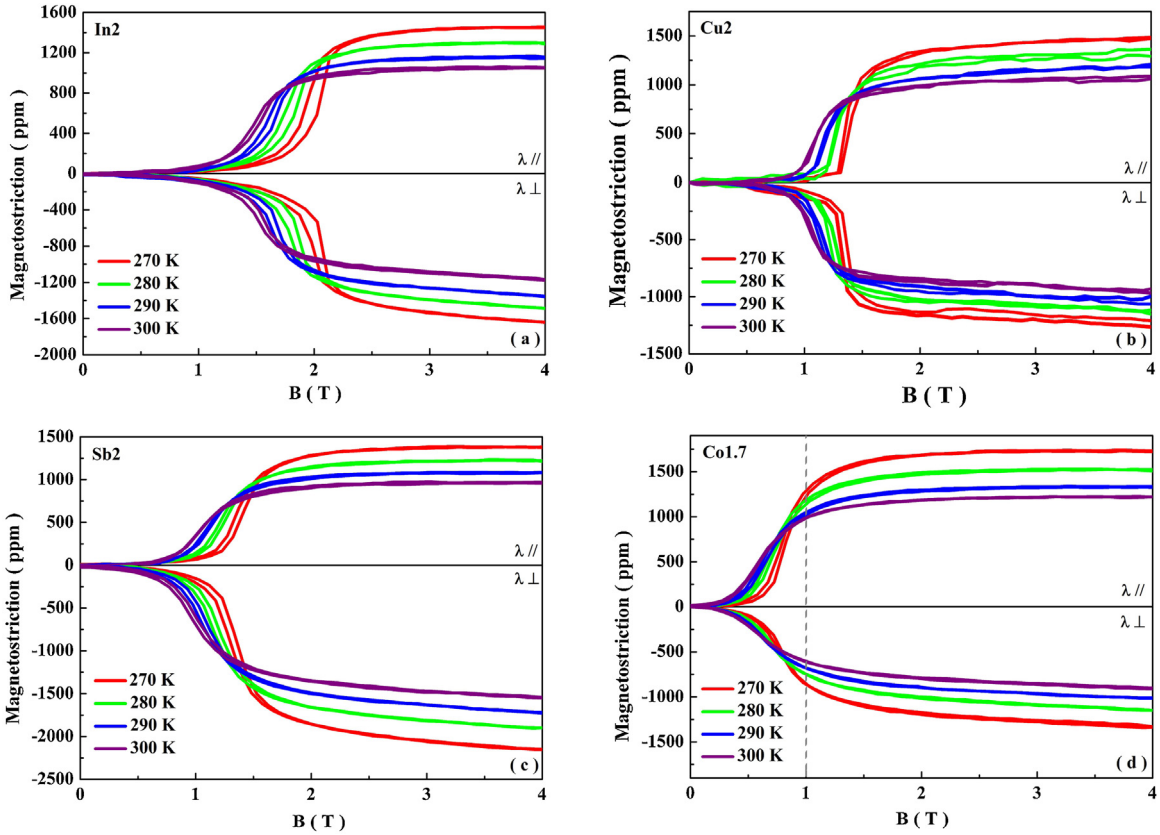

Fig. 5. The magnetostriction curves of In2 (a), Cu2 (b), Sb2 (c) and Co1.7 (d) around room temperature.

Table 3
Magnetostriction of In2, Cu2, Sb2 and Co1.7 under magnetic fields of 1 and 2 T in the temperature range of 270-300 K.

Magnetic field (T)	Temperature (K)	In2		Cu2		Sb2		Co1.7	
		λ//(ppm)	λ⊥(ppm)	λ//(ppm)	λ⊥(ppm)	λ//(ppm)	λ⊥(ppm)	λ//(ppm)	λ⊥(ppm)
1	270	18	−59	16	−82	72	−167	1226	−865
	280	31	−65	81	−110	130	−279	1140	−742
	290	50	−78	84	−159	246	−768	1029	−680
	300	81	−88	210	−308	365	−646	993	−607
2	270	580	−529	1322	−1317	1270	−1856	1690	−1184
	280	1065	−1115	1187	−1203	1150	−1659	1480	−1010
	290	1023	−1078	1062	−1056	1033	−1491	1284	−888
	300	969	−935	983	−988	917	−1348	1186	−792

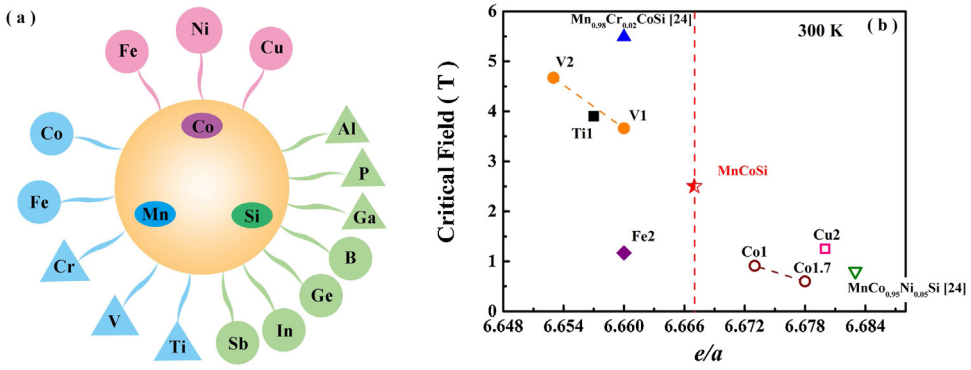

Fig. 6. (a) The effects of element substitution on B_{cri}. (b) The relationship between e/a and B_{cri} at 300 K in transition-metal-substituted MnCoSi alloys studied in this work and reported before [24]. The M-B curves of Ti1, V1 and V2 at 300 K can be found in Fig. S5 in the Supplementary Material.

-607 ppm, respectively. These values are much larger than that of the other substituted MnCoSi alloys under the same magnetic field.

4. Discussion

The effect of element substitution on B_{cri} is summarized in Fig. 6(a). Introducing the elements in a circle (triangle) intend to decrease (increase) B_{cri}. The values of B_{cri} of transition-metal-substituted MnCoSi alloys seem to be highly related to the valence electron concentration (e/a). As shown in Fig. 6(b), the increase (decrease) of e/a will lead to a decrease (an increase) of B_{cri}. Most transition-metal-substituted MnCoSi alloys obey this principle except Fe2 (Fig. 6(b)). Replacing Co with Fe reduces the B_{cri} even though the e/a is increased. The reason for this phenomenon is that replacing Co with Fe in MnCoSi lattice can construct the local Fe-6 Mn configuration, which is ferromagnetic [30,39]. It will stabilize the high magnetization state and thus reduce B_{cri}. For main-group-element-substituted MnCoSi alloys, the relation between e/a and B_{cri} is not applicable. The physical mechanism of the metamagnetic transition for these MnCoSi-based alloy needs further investigation. Additionally, we find that Sn cannot dissolve in MnCoSi alloy since the XRD patterns of $MnCoSi_{0.97}Sn_{0.03}$ alloy (Fig. S1(m) in Supplementary material) show obvious diffraction peaks of elemental Sn.

The tunable tricritical behavior of MnCoSi alloy provides a powerful tool to achieve large reversible magnetostriction under a low field. For Co1.7 alloy in this work, due to the low B_{cri} of 0.60 T at room temperature, a field of 1 T can nearly complete the metamagnetic transition, resulting in large magnetostriction shown here. Meanwhile, replacing Mn with Co can tune T_{tri} to be lower than room temperature, assuring that the room-temperature magnetostriction is generated from the second-order transition, which is reversible and hysteresis-free. These improvements overcome the drawbacks of the magnetostrain during the first-order transition, such as the high critical field and large magnetic hysteresis [11–17]. Fig. 7 summarizes the magnetostriction of slow-cooled MnCoSi-based, Fe-Ga and some other magnetic-phase-transition alloys under 1 T [4,7,11,12,14,15]. It can be found that Co1.7 exhibits a relatively larger magnetostrictive performance around room temperature. Additionally, since the B_{cri} is almost invariable between 270 and 300 K, the large magnetostriction of Co1.7 is temperature-insensitive around the ambient environment, suggesting high stability during the temperature oscillation.

However, compared with the magnetostrain originated from martensite variants reorientation in Ni-Mn-Ga single crystal [45,46], the magnetostriction is much smaller. On the other hand, MnCoSi alloy experiences a martensitic transformation at ~1190 K. The volume change during this transformation will cause spontaneous cracks in the ingots [19,25,47]. As shown in Fig. 4(a), some cracks can be observed between the columnar grains. It will reduce the measured value of magnetostriction, especially λ⊥. That is why the MnCoSi alloy displays a low λ⊥(Fig. S4 in the Supplementary material). Recently, high-magnetic-field solidification and epoxy-bonding technique have been used to obtain highly textured and dense MnCoSi sample [19,21,22]. Hence, we will adopt the two methods to further enhance the magnetostriction in Co1.7 in the next step.

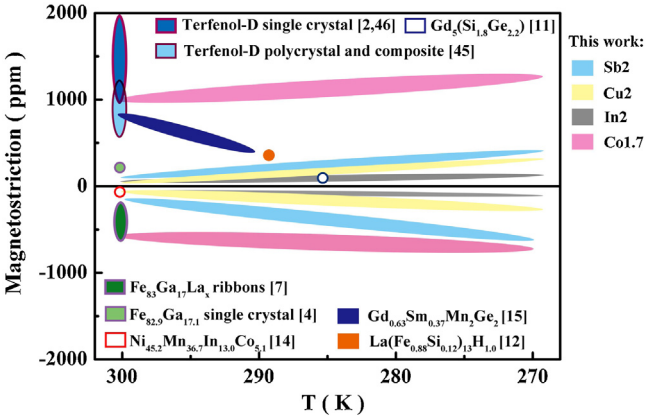

Fig. 7. A statistical graphic of the magnetostriction of MnCoSi-based, Fe-Ga and some other magnetic-phase-transition alloys under 1 T [2,4,7,11,12,14,15].

5. Conclusion

In summary, we systematically investigate the crystalline structure, metamagnetic transition, tricritical behavior and magnetostrictive effect of substituted MnCoSi alloys based on the atomic preference rule. Replacing Si with Sb or In, Co with Fe or Cu, and Mn with Co, which can reduce B_{cri} and T_{tri} simultaneously, are explored. Among the slow-cooled MnCoSi-based samples, $Mn_{0.983}Co_{1.017}Si$ shows a T_{tri} of 250 K and a room-temperature B_{cri} of 0.60 T, which is the lowest up to now. Thus, a large magnetostrictive effect is achieved at room temperature under a low field of 1 T. The obtained magnetostriction is originated from the magnetic-field-induced second-order metamagnetic transition, indicating its high reversibility and stability. Our work provides feasible ways to design MnCoSi-based alloy with large reversible magnetostriction at room temperature.

Acknowledgements

This work was financially supported by the National Natural Science Foundation of China (No. 11974184), National Natural Science Foundation of China for the Central University (No. 30919012108) and the Fundamental Research Funds for the Central Universities.

Appendix A. Supplementary data

Supplementary material related to this article can be found, in the online version, at doi:https://doi.org/10.1016/j.jmst.2020.11.011.

References

[1] J.P. Joule, Philos. Mag. 30 (1847) 76–87.
[2] A.E. Clark, Handbook of Magnetic Materials, Elsevier Science B.V., USA, 1980.
[3] D. Hunter, W. Osborn, K. Wang, N. Kazantseva, J. Hattrick-Simpers, R. Suchoski, R. Takahashi, M.L. Young, A. Mehta, L.A. Bendersky, S.E. Lofland, M. Wuttig, I. Takeuchi, Nat. Commun. 2 (2011) 1529.
[4] H.D. Chopra, M. Wuttig, Nature 521 (2015) 340–343.
[5] A.E. Clark, J.P. Teter, O.D. McMasters, J. Appl. Phys. 63 (1988) 3910–3912.
[6] S. Guruswamy, N. Srisukhumbowornchai, A.E. Clark, J.B. Restorff, M. Wun-Fogle, Scr. Mater. 43 (2000) 239–244.
[7] Y.K. He, C.B. Jiang, W. Wu, B. Wang, H.P. Duan, H. Wang, T.L. Zhang, J.M. Wang, J.H. Liu, Z.L. Zhang, P. Stamenov, J.M.D. Coey, H.B. Xu, Acta Mater. 109 (2016) 177–186.
[8] T.Y. Ma, J.M. Gou, S.S. Hu, X.L. Liu, C. Wu, S. Ren, H. Zhao, A.D. Xiao, C.B. Jiang, X.B. Ren, M. Yan, Nat. Commun. 8 (2017) 13937.
[9] S.A. Wilson, R.P.J. Jourdain, Q. Zhang, R.A. Dorey, C.R. Bowen, M. Willander, Mater. Sci. Eng. R 56 (2007) 1–129.
[10] A.G. Olabi, A. Grunwald, Mater. Des. 29 (2008) 469–483.
[11] L. Morellon, P.A. Algarabel, M.R. Ibarra, J. Blasco, B. García-Landa, Z. Arnold, Phys. Rev. B 58 (1998) R14721–R14724.
[12] S. Fujieda, A. Fujita, K. Fukamichi, Y. Yamazaki, Y. Iijima, Appl. Phys. Lett. 79 (2001) 653–655.
[13] U. Gaitzsch, M. Pötschke, S. Roth, B. Rellinghaus, L. Schultz, Acta Mater. 57 (2009) 365–370.
[14] J. Liu, S. Aksoy, N. Scheerbaum, M. Acet, O. Gutfleisch, Appl. Phys. Lett. 95 (2009) 232515.
[15] Y.Y. Gong, L. Zhang, Q.Q. Cao, D.H. Wang, Y.W. Du, J. Alloys. Compd. 628 (2015) 146–150.
[16] Q.B. Hu, Y. Hu, Y. Fang, D.H. Wang, Q.Q. Cao, Y.T. Yang, J. Li, Y.W. Du, AIP Adv. 7 (2017) 056430.
[17] X.M. Sun, D.Y. Cong, Z. Li, Y.L. Zhang, Z. Chen, Y. Ren, K.D. Liss, Z.Y. Ma, R.G. Li, Y.H. Qu, Z. Yang, L. Wang, Y.D. Wang,Phys. Rev. Mater. 3 (2019), 034404.
[18] A. Barcza, Z. Gercsi, K.S. Knight, K.G. Sandeman,Phys. Rev. Lett. 104 (2010), 247202.
[19] Y.Y. Gong, D.H. Wang, Q.Q. Cao, Y.W. Du, T. Zhi, B.C. Zhao, J.M. Dai, Y.P. Sun, H.B. Zhou, Q.Y. Lu, J. Liu, Acta Mater. 98 (2015) 113–118.
[20] Y.Y. Gong, J. Liu, G.Z. Xu, F. Xu, D.H. Wang, Scr. Mater. 127 (2017) 165–168.
[21] Q.B. Hu, Y. Hu, S. Zhang, W. Tang, X.J. He, Z. Li, Q.Q. Cao, D.H. Wang, Y.W. Du, Appl. Phys. Lett. 112 (2018) 052404.
[22] C.L. Zhang, H.F. Shi, Y.G. Nie, E.J. Ye, J.H. Wen, Z.D. Han, D.H. Wang, J. Alloys Compd. 784 (2019) 16–21.
[23] K. Morrison, J.D. Moore, K.G. Sandeman, A.D. Caplin, L.F. Cohen,Phys. Rev. B 79 (2009), 134408.
[24] A. Barcza, Z. Gercsi, H. Michor, K. Suzuki, W. Kockelmann, K.S. Knight, K.G. Sandeman, Phys. Rev. B 87 (2013) 064410.
[25] J. Liu, Y. Si, Y.Y. Gong, G.Z. Xu, E. Liu, F. Xu, J. Alloys Compd. 701 (2017) 858–863.
[26] K.G. Sandeman, R. Daou, S. Özcan, J.H. Durrell, N.D. Mathur, D.J. Fray,Phys. Rev. B 74 (2006), 224436.
[27] K. Morrison, Y. Miyoshi, J.D. Moore, A. Barcza, K.G. Sandeman, A.D. Caplin,Phys. Rev. B 78 (2008), 134418.
[28] Y.D. Zavorotnev, L.I. Medvedeva, B.M. Todris, E.A. Dvornikov, O.Yu.J. Magn, Magn. Mater. 323 (2011) 2808–2812.
[29] A. Szytula, A.T. Pedziwiatr, Z. Tomkowicz, W. Bażeła, J. Magn. Magn. Mater. 25 (1981) 176–186.
[30] E.K. Liu, W.H. Wang, L. Feng, W. Zhu, G.J. Li, J.L. Chen, H.W. Zhang, G.H. Wu, C.B. Jiang, H.B. Xu, F. de Boer, Nat. Commun. 3 (2012) 873.
[31] J. Liu, Y.Y. Gong, Y.R. You, X.M. You, B.H. Huang, X.F. Miao, G.Z. Xu, F. Xu, E. Brück, Acta Mater. 174 (2019) 450–458.
[32] J. Liu, Y.R. You, I. Batashev, Y.Y. Gong, X.M. You, B.W. Huang, F.Q. Zhang, X.F. Miao, F. Xu, N. van Dijk, E. Brück, Phys. Rev. Appl. 13 (2020) 054003.
[33] T. Samanta, D.L. Lepkowski, A.U. Saleheen, A. Shankar, J. Prestigiacomo, I. Dubenko, A. Quetz, I.W.H. Oswald, G.T. McCandless, J.Y. Chan, P.W. Adams, D.P. Young, N. Ali, S. Stadler, Phys. Rev. B 91 (2015), 020401(R).
[34] Z.Y. Wei, E.K. Liu, Y. Li, G.Z. Xu, X.M. Zhang, G.D. Liu, X.K. Xi, H.W. Zhang, W.H. Wang, G.H. Wu, X.X. Zhang, Adv. Electron. Mater. 1 (2015) 1500076.
[35] J. Liu, Y.Y. Gong, G.Z. Xu, G. Peng, I.A. Shah, N. ul Hassan, F. Xu, Sci. Rep. 6 (2016) 23386.
[36] O. Beckman, L. Lundgren, Handbook of Magnetic Materials, vol. 6, Elsevier Science B.V., USA, 1991.
[37] G.A. Landrum, R. Hoffmann, J. Evers, H. Boysen, Inorg. Chem. 37 (1998) 5754–5763.
[38] J.H. Xu, W.Y. Yang, Q.H. Du, Y.H. Xia, H.L. Du, J.B. Yang, C.S. Wang, J.Z. Han, S.Q. Liu, Y. Zhang, Y.C. Yang, J. Phys. D-Appl. Phys. 47 (2014) 065003.
[39] J.H. Chen, Z.Y. Wei, E.K. Liu, X. Qi, W.H. Wang, G.H. Wu, J. Magn. Magn. Mater. 387 (2015) 159–164.
[40] Z. Gercsi, K.G. Sandeman, Phys. Rev. B 81 (2010) 224426.
[41] Z. Gercsi, K. Hono, K.G. Sandeman, Phys. Rev. B 83 (2010) 174403.
[42] J.B. Staunton, M. dos Santos Dias, J. Peace, Z. Gercsi, K.G. Sandeman, Phys. Rev. B 87 (2013), 060404(R).
[43] K. Morrison, A. Barcza, J.D. Moore, K.G. Sandeman, M.K. Chattopadhyay, S.B. Roy, A.D. Caplin, L.F. Cohen, J. Phys. D-Appl. Phys. 43 (2010) 195001.
[44] K. Ullakko, Y. Ezer, A. Sozinov, G. Kimmel, P. Yakovenko, V.K. Lindroos, Scr. Mater. 44 (2001) 475–480.
[45] C. Jiang, T. Liang, H. Xu, M. Zhang, G. Wu, Appl. Phys. Lett. 81 (2002) 2818.
[46] C. Jiang, J. Wang, H. Xu, Appl. Phys. Lett. 86 (2005) 252508.
[47] V. Johnson, Inorg. Chem. 14 (1975) 1117–1120.